A Base Change in the Catalytic Core of the Hairpin Ribozyme Perturbs Function but Not Domain Docking†

Nils G. Walter,*,‡,§ Philip A. Chan,§ Ken J. Hampel,§ David P. Millar,|| and John M. Burke§

Department of Chemistry, The University of Michigan, Ann Arbor, Michigan 48109-1055, Markey Center for Molecular Genetics, Department of Microbiology and Molecular Genetics, The University of Vermont, Burlington, Vermont 05405, and Department of Molecular Biology (MB-19), The Scripps Research Institute, 10550 North Torrey Pines Road, La Jolla, California 92037

Received July 11, 2000; Revised Manuscript Received December 19, 2000

ABSTRACT: The hairpin ribozyme is a small endonucleolytic RNA motif with potential for targeted RNA inactivation. It optimally cleaves substrates containing the sequence 5′-GU-3′ immediately 5′ of G. Previously, we have shown that tertiary structure docking of its two domains is an essential step in the reaction pathway of the hairpin ribozyme. Here we show, combining biochemical and fluorescence structure and function probing techniques, that any mutation of the substrate base U leads to a docked RNA fold, yet decreases cleavage activity. The docked mutant complex shares with the wild-type complex a common interdomain distance as measured by time-resolved fluorescence resonance energy transfer (FRET) as well as the same solvent-inaccessible core as detected by hydroxyl-radical protection; hence, the mutant complex appears nativelike. FRET experiments also indicate that mutant docking is kinetically more complex, yet with an equilibrium shifted toward the docked conformation. Using 2-aminopurine as a site-specific fluorescent probe in place of the wild-type U, a local structural rearrangement in the substrate is observed. This substrate straining accompanies global domain docking and involves unstacking of the base and restriction of its conformational dynamics, as detected by time-resolved 2-aminopurine fluorescence spectroscopy. These data appear to invoke a mechanism of functional interference by a single base mutation, in which the ribozyme−substrate complex becomes trapped in a nativelike fold preceding the chemical transition state.

Much like a protein, an RNA needs to fold into a complex tertiary structure, its native state, to acquire biological function. Unlike the protein folding problem, however, the question of how an RNA sequence specifies a unique fold has only recently attracted increasing attention (*1*−*4*). Recent structural studies have revealed that large RNAs often fold in a quasi-hierarchical manner (*3*); a kinetically favored secondary or partial tertiary structure forms first but is rearranged by the formation of competing long-range tertiary interactions. In some cases, this rearrangement has high activation energy, so as to kinetically trap the RNA on its folding pathway to the lower-energy tertiary structure. In contrast to most proteins, a change in a single RNA residue can either relieve such a kinetic folding trap (*5*−*7*) or prevent tertiary folding altogether (*8*−*10*).

Convenient model systems to study RNA folding are ribozymes, since their catalytic function readily reports the presence of a folded native structure. The hairpin ribozyme is a small endonucleolytic RNA motif that has proven to be both a model for RNA folding problems (*3*, *8*−*13*) as well as a gene therapeutic agent for targeted RNA inactivation (*13*, *14*). From the naturally occurring RNA four-way junction, it has been engineered into a hinged two-way junction that optimally cleaves external substrates of the sequence 5′-GU-3′ immediately 5′ of G (*11*). This minimal ribozyme−substrate complex consists of the two helix−loop−helix domains A and B that approach each other to dock into the catalytically active form [Figure 1(a)]. High-resolution NMR[1] structures of the isolated domains have been determined (*15*, *16*), and domain docking has been studied by steady-state and time-resolved fluorescence resonance energy transfer (FRET) (*8*, *10*, *12*), hydroxyl-radical footprinting (*9*), interdomain cross-linking (*17*, *18*), and molecular modeling (*17*, *19*). Recent studies have revealed a functionally crucial Watson−Crick base pair between G+1 of the substrate and C25 of the ribozyme core, an interaction that might guide proper alignment of the two domains [Figure 1(a)] (*19*). To accommodate this G+1/C25 pair in the active complex, a significant rearrangement from the solution structures of the isolated domains has to be assumed, suggesting that they dock by induced fit of the ribozyme (*19*) and possibly straining of the substrate (*20*). Such a

† This work was supported by grants from the National Institutes of Health to D.P.M. and J.M.B.

* To whom correspondence should be addressed at The University of Michigan. Phone: (734)615-2060. Fax: (734)647-4865. Email: nwalter@umich.edu.

‡ The University of Michigan.

§ The University of Vermont.

|| The Scripps Research Institute.

[1] Abbreviations: ab, abasic site with 2′-deoxyribose; AP, 2-aminopurine; dT, deoxythymidine; EDTA, ethylenediaminetetraacetic acid; FRET, fluorescence resonance energy transfer; HPLC, high-performance liquid chromatography; I, inosine; NMR, nuclear magnetic resonance; WT, wild-type.

10.1021/bi001609f CCC: $20.00
Published on Web 02/01/2001

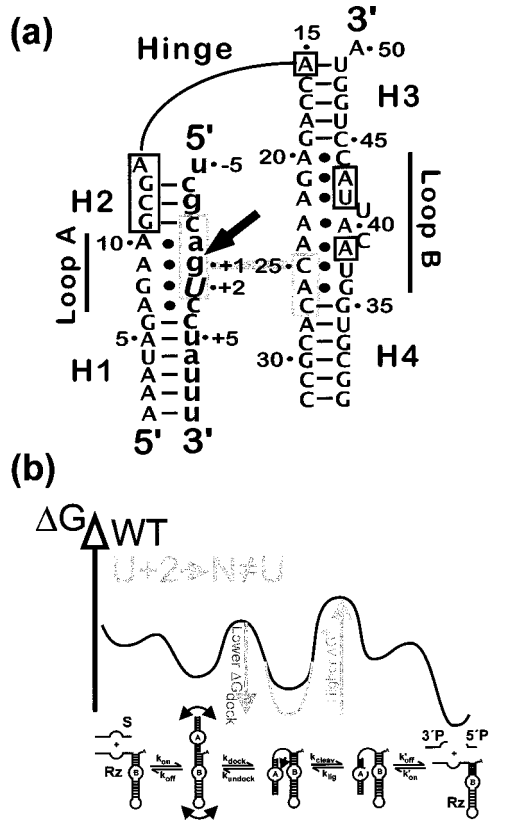

FIGURE 1: Folding and activity of the hairpin ribozyme. (a) Schematic of known secondary and tertiary structure elements of the hairpin ribozyme−substrate complex. The 2-strand hairpin ribozyme used in this study binds its 14-nucleotide substrate (small letters; arrow, cleavage site) to form domain A, comprising helices H1 and H2 (short lines, Watson−Crick base pairs) and the symmetric internal loop A. For structural studies, cleavage was chemically blocked by a 2′-deoxy modification of the ribose immediately upstream of the cleavage site. The substrate binding domain A is connected via a flexible hinge to the B domain of the ribozyme containing helices H3 and H4 and the asymmetric internal loop B. Noncanonical base pairs are indicated as dots (*15, 16*). Regions boxed in the same shade become co-protected from hydroxyl radicals and are likely to interact in the internalized catalytic core of the ribozyme−substrate complex (*9, 18*). G+1 of the substrate and C25 of loop B interact in a crucial Watson−Crick type base pair (gray line) (*19*). Here, we investigate how substitutions of the adjacent U+2 (capital italics) interfere with activity. (b) Simplified model for free energy changes in the reaction pathway of the hairpin ribozyme. Substrate (S) is bound by the ribozyme (Rz) to form an extended complex, with helices H2 and H3 coaxially stacked (*8, 30*). This inactive intermediate, posing a kinetic trap, needs to dock into the more stable form in which loops A and B interact, preceding the chemical transition state (‡) (*8, 10*). The cleaved docked complex is less stable than the intact one, potentially leading to re-ligation of the cleavage products (*37, 38*). However, the short 5′ and 3′ products (5′P, 3′P) generated during cleavage lead to undocking and energetically favorable dissociation of the complex. In the current study, we found mutations of substrate base U+2 to result in stabilization of a docked ribozyme−substrate complex, offering a plausible explanation for the observed higher transition state free energy ($\Delta G^{\ddagger}$) (gray).

significant structural rearrangement is also consistent with the high activation energy associated with domain docking (*8*).

Here, we have studied the role in docking and catalytic activity of the conserved substrate base U+2, located next to G+1 in the core of the docked ribozyme−substrate complex (*21*−*23*). All tested modifications of this base, except for a substitution with deoxy-T, lead to substantial activity loss. The tertiary structure of the modified complex, however, shows the same interdomain distance (as measured by time-resolved fluorescence resonance energy transfer) and solvent-inaccessible core (as detected by hydroxyl-radical protection) as the docked conformer of the unmodified complex. In fact, modified complexes dock stably, yet with more complex kinetics than the wild-type complex. Using 2-aminopurine as a site-specific fluorescent probe in place of U+2, a local structural rearrangement is observed. This conformational transition is part of the substrate straining or mutually induced fit associated with domain docking and involves unstacking of the +2 base and restriction of its conformational dynamics. These data invoke a mechanism of functional interference by a single base mutation, in which the ribozyme−substrate complex becomes trapped in a nativelike fold preceding the chemical transition state [Figure 1(b)].

MATERIALS AND METHODS

RNA Preparation. RNA was synthesized on an Applied Biosystems 392 DNA/RNA synthesizer, using standard solid-phase phosphoramidite chemistry (Glen Research). A three-strand ribozyme−substrate complex (ribozyme strand A, 5′-AAAUAGAGAAGCGAACCAGAGAAACACACGCC-3′; ribozyme strand B, 5′-GGCGUGGUACAUUACCUG-GUA-3′; wild-type substrate strand, 5′-UCGCAG***U***CCUA-UUU-3′; the latter was modified with 2′-deoxy at the underlined adenosine to obtain a chemically blocked, non-cleavable substrate analogue for all structural analyses; mutant substrates and their noncleavable analogues were obtained by substituting the boldface italic U) was used throughout all studies, except footprinting. For kinetic FRET assays, the 5′ and 3′ ends of ribozyme strand A were labeled with hexachlorofluorescein and fluorescein, respectively (*8*), while trFRET analysis required fluorescein and tetramethylrhodamine as 5′- and 3′-end labels (*10*), respectively. To simplify analysis of hydroxyl-radical footprinting data, the noncleavable substrate analogue was connected with the ribozyme through a six nucleotide linker of sequence ACCCCC, generating a two-strand complex. 2-Aminopurine and inosine nucleosides were incorporated using their commercially available 2′-*O*-methyl phosphoramidites (Glen Research). Oligonucleotides were deprotected with ethanolic ammonia and triethylamine trihydrofluoride and purified by denaturing 20% polyacrylamide, 8 M urea gel electrophoresis and C_8-reverse-phase HPLC chromatography as described (*24*).

Cleavage Reactions. 5′-^{32}P-labeled substrate was prepared by phosphorylation with T4 polynucleotide kinase and [γ-^{32}P]-ATP. After preincubation for 15 min at the temperature of choice, a trace ($\leq$1 nM) amount of 5′-^{32}P-labeled substrate was added to a saturating concentration of 100 nM ribozyme in standard buffer (50 mM Tris-HCl, pH 7.5, 12 mM $MgCl_2$), and aliquots were taken and stopped by addition of 25 mM EDTA in 80% formamide. The 5′ cleavage product was separated from uncleaved substrate by denaturing 20% polyacrylamide gel electrophoresis, and was quantified and normalized to the sum of the substrate and product bands using a Bio-Rad Molecular Imager System GS-525 (*8*). The time trace of product formation was fitted to the single-exponential equation: $y = y_0 + A_1(1 - e^{-t/\tau 1})$, except for some of the faster cleavage reactions that required double-

exponential fits: $y = y_0 + A_1(1 - e^{-t/\tau 1}) + A_2(1 - e^{-t/\tau 2})$ (as judged by careful examination of the residuals and a substantial improvement in the goodness-of-fit χ^2), employing Marquardt−Levenberg nonlinear least-squares regression (Microcal Origin). In the latter case, the fast-phase component contributed at least 75% to the overall extent of cleavage, while the slow-phase rate constant likely reflects dissociation of substrate from an inactive ribozyme−substrate conformer (*25*) and was disregarded for this study.

Kinetic FRET Measurements. Steady-state FRET measurements of RNA doubly labeled with hexachlorofluorescein and fluorescein were performed as previously described (*8*). Briefly, 200 nM annealed ribozyme (with a 2-fold excess of the unlabeled 3′-segment) was incubated in a 150 μL cuvette for at least 15 min at 25 °C in standard buffer supplemented with 25 mM dithiothreitol. The ribozyme−substrate complex was rapidly formed by addition of 2 μM noncleavable substrate analogue. Fluorescein was excited at 485 nm (4 nm bandwidth), and fluorescence emission was recorded simultaneously at the fluorescein (515 nm) and hexachlorofluorescein (560 nm, 8 nm bandwidth) wavelengths in an Aminco-Bowman Series 2 (AB2) spectrofluorometer (Spectronic). A ratio $Q = F_{560}/F_{515}$ was calculated and normalized with its starting value to reflect the relative FRET efficiency. The resulting growth curves were fitted, similar as described for the cleavage kinetics, to the single-exponential function $y = y_0 + A_1(1 - e^{-t/\tau 1})$, or, if this approach failed to give a good fit (as judged by the χ^2 value and inspection of residuals), to the double-exponential function $y = y_0 + A_1(1 - e^{-t/\tau 1}) + A_2(1 - e^{-t/\tau 2})$, yielding docking rate constants $k_i = 1/\tau_i$ and amplitudes A_i.

TrFRET Measurements. The global structure of the ribozyme−substrate complex was studied by trFRET analysis of a ribozyme−substrate complex doubly labeled with fluorescein and tetramethylrhodamine, as previously described (*10*). In short, the annealed ribozyme−substrate complex (150 μL, 1 μM doubly labeled 5′-ribozyme segment and 3 μM each of 3′-segment and noncleavable substrate analogue) was incubated at 17.8 °C for at least 15 min in standard buffer, prior to collecting time-resolved emission profiles of the fluorescein donor using time-correlated single photon counting as described (*26*). Pulsed excitation from a mode-locked argon ion laser was at 514 nm, and isotropic emission detection to >40 000 peak counts (2048 sampling channels) was performed under magic angle conditions at 530 nm (16 nm slit width plus 530 nm cutoff filter). To derive distance information, two time-resolved fluorescence decays were collected, with and without acceptor in place. The effect of the acceptor on the decay of fluorescein emission in the doubly labeled complex was extracted using a model for two three-dimensional Gaussian distance distributions of the two fluorophores (*10, 26*). To calculate distances, a value of 2/3 for the orientation factor was assumed and experimentally supported by the observation of large-amplitude rotational motions of both fluorescein and tetramethylrhodamine (*10*).

2-Aminopurine Fluorescence Measurements. A 150 μL aliquot of 400 nM noncleavable substrate analogue with 2-aminopurine as fluorescent probe was incubated for at least 15 min at 25 °C in standard buffer, or with varying Mg^{2+} concentrations, prior to addition of a 3-fold excess of ribozyme (reconstituted from stoichiometric amounts of 5′- and 3′-segment). For steady-state measurements, 2-aminopurine was excited at 320 nm (8 nm bandwidth), and fluorescence emission was recorded at 380 nm (8 nm bandwidth). The emission signal was normalized with its value immediately after formation of the ribozyme−substrate complex, and the resulting growth curves were fitted with the double-exponential function $y = y_0 + A_1(1 - e^{-t/\tau 1}) + A_2(1 - e^{-t/\tau 2})$ as described for the kinetic FRET assay. The Mg^{2+} dependence of the fast rate constant was fitted to the cooperative binding equation:

$$k = k_{max}\frac{[Mg^{2+}]^n}{[Mg^{2+}]^n + K_D{}^n}$$

to yield an apparent Mg^{2+} dissociation constant, K_D, and a cooperativity coefficient, n (*8*).

Fluorescence decay profiles were recorded by time-correlated single photon counting. Samples [150 μL, 1 μM noncleavable substrate analogue and 3 μM ribozyme at 25 °C in either standard buffer ("$+Mg^{2+}$") or substituting 100 mM NaCl for Mg^{2+} ("$-Mg^{2+}$") for secondary structure formation in the absence of tertiary structure] were excited at 317 nm with the frequency-doubled output of a mode-locked dye laser pumped by an argon-ion laser, as previously described (*27*). Isotropic emission detection to about 40 000 peak counts (2048 sampling channels) was performed under magic angle conditions at 410 nm (4 nm slit width). The time-dependent emission anisotropy was measured by accumulating two separate decay curves, one obtained with the emission polarizer set in the vertical direction and the other set in the horizontal direction. The obtained emission and anisotropy decay data were deconvoluted with the instrument response function as described (*27*) and fitted with a single- or multi-exponential decay function of the form $y = A_1e^{-t/\tau 1} + A_2e^{-t/\tau 2} + ...$ similar as described above, yielding decay time constants τ_i and amplitudes A_i.

Hydroxyl-Radical Footprinting. The solvent-protected core of the ribozyme−substrate complex was characterized with single-nucleotide resolution by hydroxyl-radical footprinting using Fenton chemistry, as previously described (*9*). Briefly, 30 nM 5′-end-labeled RNA and 200 nM unlabeled RNA were annealed for 20 min at 25 °C in 25 mM sodium cacodylate, pH 7.1, 100 mM NaCl, in the absence or presence of either 12 mM Mg^{2+} or 1.5 mM $Co(NH_3)_6{}^{3+}$. One microliter each of 0.4% v/v H_2O_2, 50 mM sodium ascorbate, and Fe(II)-EDTA [10 mM $Fe(NH_4)_2(SO_4)_2$ and 12 mM EDTA, pH 8.0, mixed immediately before] was pipetted separately to the wall of the reaction tube. The reaction was initiated by spinning these solutions into the RNA solution, allowed to proceed for 3 min in the dark at room temperature, and terminated by addition of 10 mM thiourea, 90% formamide, 0.02% bromophenol blue, and 0.02% xylene cyanol. Products were analyzed on wedged 10% polyacrylamide, 8 M urea sequencing gels.

RESULTS AND DISCUSSION

Substrate Base U+2 Is Catalytically Important. Loss of activity in a catalytic RNA upon introduction of a specific modification can be caused by either interference with structure formation or reaction chemistry. It is often difficult to distinguish these alternatives. For example, in the hairpin

Table 1: Cleavage Rate Constants and Activation Parameters for Mutant Substrates[a]

mutation[b]	k_{cleav} (min^{-1})	$\Delta G^{\ddagger}$ (kcal/mol)	$\Delta H^{\ddagger}$ (kcal/mol)	$\Delta S^{\ddagger}$ (eu)
WT	0.12 ± 0.03	21	21	0.6
U+2→dT	0.13 ± 0.03	nd[c]	nd[c]	nd[c]
U+2→ab	0.015 ± 0.002	22	18	−16
U+2→C	0.0017 ± 0.0005	24	23	−2.0
U+2→A	0.0089 ± 0.0009	23	23	0.5
U+2→G	0.0030 ± 0.0005	23	22	−5.1
U+2→AP	0.0035 ± 0.0005	23	24	1.7
U+2→I	0.0045 ± 0.0007	23	20	−12

[a] Cleavage rate constants k_{cleav} were measured under standard conditions: 50 mM Tris-HCl, pH 7.5, 12 mM $MgCl_2$, 25 °C, with errors from at least two independent determinations. Activation parameters were calculated for $T = 298.15$ K (25 °C) from $\Delta G^{\ddagger} = -RT \ln(k_{cleav}h/k_BT)$, where h is Planck's constant and k_B is Boltzmann's constant; $\Delta H^{\ddagger} = E_a - RT$, with the activation energy E_a derived from Arrhenius plots over a range of six temperatures from 10 to 37 °C; and $\Delta S^{\ddagger} = (\Delta H^{\ddagger} - \Delta G^{\ddagger})/T$; we estimate the errors on $\Delta G^{\ddagger}$, $\Delta H^{\ddagger}$, and $\Delta S^{\ddagger}$ values to 10% or less. [b] dT = 2′-deoxythymidine; ab = abasic site with 2′-deoxyribose; C = cytidine; A = adenosine; G = guanosine; AP = 2-aminopurine with 2′-*O*-methylribose; I = inosine with 2′-*O*-methylribose. [c] nd = not determined.

ribozyme, a catalytically deleterious mutation of substrate base G+1 initially was suggested to interfere with reaction chemistry (*28*), but later was found to also impair folding into the native structure (*8*−*10*, *19*). To achieve a deeper understanding of structure−function relationships in the hairpin ribozyme, we developed an array of structure probing techniques to complement our functional analyses. Using these techniques, we were not able to confirm an earlier result indicating that specifically the 2-amino group of G+1 is an essential component of the active site during catalysis (*28*). In contrast, we found that any mutation at position +1, including the guanine analogue 2-aminopurine, impairs docking of the ribozyme−substrate complex and leads to at least 30-fold lower catalytic activity, in the context of three widely utilized ribozyme−substrate constructs (*25*, *28*, *29*) (data not shown).

This result prompted us to study in detail the functional role of the only other conserved substrate base, U+2, in the catalytic core of the ribozyme−substrate complex [Figure 1(a)]. Characterization of substrates carrying a number of base substitutions in position +2, under standard buffer conditions (50 mM Tris-HCl, pH 7.5, 12 mM Mg^{2+}) and at varying temperature, yielded the cleavage rate constants and activation parameters reported in Table 1. In good agreement with earlier findings (*21*−*23*, *28*), substitution of the natural bases C, A, or G for U+2 leads to a 70-fold, 13-fold, and 40-fold decrease in the cleavage rate constant at 25 °C, respectively. Likewise, substitution with the guanine analogues 2-aminopurine (AP) and inosine (I) yields rate constants 34-fold and 27-fold lower than that for the wild-type substrate, respectively. In most cases, the effect can primarily be attributed to an increase in the transition state enthalpy, $\Delta H^{\ddagger}$, while the transition state entropy, $\Delta S^{\ddagger}$, remains low, as is that of the wild-type substrate (Table 1). When converting the +2 position into an abasic site with a 2′-deoxyribose (ab), however, the 8-fold reduction in rate constant is primarily due to a high negative transition state entropy $\Delta S^{\ddagger}$, supporting the notion of a change in the rate-limiting step (see below). The only modification of position +2 that does not interfere with cleavage activity is a substitution with deoxythymidine (dT, Table 1), introducing subtle 5-methyl and 2′-deoxy modifications.

U+2 Substitutions Lead to a Stably Docked Ribozyme−*Substrate Complex.* While our cleavage results confirm and expand previous functional data, the key to their understanding is to probe the involved secondary and tertiary structures. Previously, we have found that substrate binding and dissociation in U+2 mutant ribozyme−substrate complexes occur with similar rate constants (e.g., 0.8×10^8 M^{-1} min^{-1} and 0.025 min^{-1}, respectively, for U+2→G) as in the wild-type complex (*30*, and data not shown). In addition, our cleavage data were obtained under single-turnover conditions, with ribozyme in saturating concentration. Thus, we can rule out that slow secondary structure formation is responsible for the observed slower cleavage of U+2 mutant substrates.

Tertiary structure formation can be directly observed as an increase in the relative fluorescence resonance energy transfer (FRET) efficiency by labeling the termini of domains A and B with a donor/acceptor fluorophore pair (see Materials and Methods) (*8*). As previously observed (*8*), docking after addition of the wild-type (WT) substrate leads to a single-exponential FRET increase with an apparent rate constant of 0.70 ± 0.08 min^{-1} (Figure 2). Likewise, docking of the catalytically proficient U+2→dT mutant substrate gives rise to a slightly faster (1.22 ± 0.08 min^{-1}), single-exponential FRET increase [note that the apparent rate constant is a composite of the elementary docking and undocking rate constants (*8*)].

In contrast, the U+2→ab mutant substrate does not lead to a detectable level of docked conformation, showing that domain docking is extremely slow and/or unfavorable for this mutant (Figure 2). Taken together with the high negative transition state entropy $\Delta S^{\ddagger}$ of its rate-limiting step (Table 1), this observation suggests that domain docking, which is associated with a high entropic cost (*31*), may become partially limiting for the observed cleavage rate of the U+2→ab mutant substrate.

All other substrates with base substitutions of U+2 are very efficient in FRET-detected docking (Figure 2). In fact, docking clearly occurs in two phases, a major fast phase with rate constants comparable to those of the WT substrate, and a 4−26-fold slower phase of low extent (6−27%, Figure 2; the contributions of the fast phases alone are indicated as dashed lines). The two simplest explanations for this observation are, first, that two kinetically distinct populations of docked ribozyme−substrate complexes exist or, second, that all mutant ribozyme−substrate complexes undergo a two-step docking mechanism. In either case, the mutant complexes may well be structurally distinct from the WT substrate containing one. To detect such differences, we analyzed the donor−acceptor distance in the mutant complex with the most pronounced double-exponential docking kinetics, the U+2→G modified one, by time-resolved FRET (*10*) (trFRET; see Materials and Methods). We found the donor−acceptor distance distributions of the extended and docked conformers to be indistinguishable for the WT and mutant ribozyme−substrate complexes. However, the relative abundance of docked complex increased from 65 ± 1% to 81 ± 1% upon introduction of the U+2→G mutation [Figure 3-(a)], indicating an additional thermodynamic stabilization of the mutant docked complex by about 0.5 kcal/mol, well above the detection limit of trFRET (*10*).

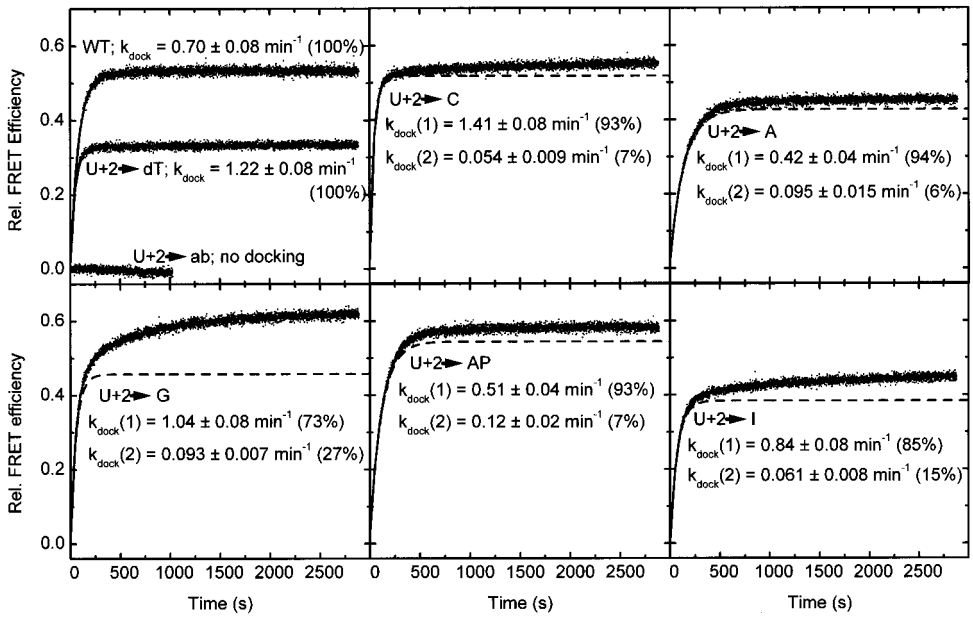

FIGURE 2: Analysis of the docking kinetics of mutant hairpin ribozyme−substrate complexes by fluorescence resonance energy transfer (FRET). After formation of the ribozyme−substrate complex (containing noncleavable substrate analogues) under standard conditions (50 mM Tris-HCl, pH 7.5, 12 mM $MgCl_2$, 25 °C), the relative FRET efficiency between a domain terminal fluorophore pair was observed; the increase in relative FRET efficiency upon domain docking (scatter) was fitted to single- and double-exponential growth functions (solid lines; see Materials and Methods) (*8*). For the complexes with the wild-type (WT) and the U+2→dT mutant substrate analogues, double-exponential fits improved the χ^2 value by less than 20% as compared to single-exponential fits, and indicated less than 5% contribution of a second phase. Double-exponential fits for the mutant complexes, however, typically improved χ^2 by at least 50% compared to single-exponentials. Fitting results are presented as docking rate constants k_{dock} (with errors from comparing at least three independent determinations) with their relative amplitudes in parentheses (with errors estimated to ±2% from at least three independent determinations). Dashed lines, contributions of the fast-phase components that alone cannot satisfy the data.

Table 2: Fluorescence Intensity and Fluorescence Anisotropy Decay Times of Substrates Containing 2-Aminopurine (AP)

	intensity decay times (ns)[a]				anisotropy decay times (ns)[b]	
mutation	τ1	τ2	τ3	τ4	τ1 [χ^2]	τ1, τ2 [χ^2]
U+2→(AP) + Mg^{2+}	0.086 (23%)	1.00 (10%)	4.39 (28%)	10.0 (39%)	15.4 [1.13]	0.03 (<0.1%), 15.4 (>99.9%) [1.13]
U+2→(AP) − Mg^{2+}	0.094 (38%)	1.00 (20%)	3.53 (35%)	8.38 (7%)	9.22 [1.71]	0.42 (21%), 10.9 (79%) [1.18]
G+1→(AP) + Mg^{2+}	0.091 (41%)	0.75 (30%)	2.47 (22%)	8.33 (7%)	nd[c]	nd[c]
G+1→(AP) − Mg^{2+}	0.089 (39%)	0.72 (30%)	2.40 (23%)	8.55 (8%)	nd[c]	nd[c]
A-1→(AP) + Mg^{2+}	0.056 (80%)	0.42 (11%)	2.88 (5%)	9.16 (4%)	nd[c]	nd[c]
A-1→(AP) − Mg^{2+}	0.045 (82%)	0.34 (11%)	2.56 (4%)	8.85 (3%)	nd[c]	nd[c]

[a] Fluorescence decay data for 2-aminopurine coupled to RNA have to be fitted with four lifetimes (*27*), with their relative contributions given in parentheses; errors are estimated to ±0.005 ns for τ1, ±0.04 ns for τ2, ±0.05 ns for τ3, ±0.10 ns for τ4, and ±2% for the amplitudes. [b] Fluorescence anisotropy decay data for 2-aminopurine were fitted allowing for one and two lifetimes (relative contributions given in parentheses), respectively, and the goodness of these fits was compared by inspecting their χ^2 values; a single-exponential fit suffices for the "+Mg^{2+}" data, while a second exponential is required for a low χ^2 in case of the "−Mg^{2+}" data set [Figure 4(c)]; errors are estimated to ±0.02 and ±0.2 ns for the fast and slow lifetime components, respectively, and ±2% for the amplitudes. [c] nd = not determined.

Next, we compared the WT and U+2→G mutant ribozyme−substrate complexes in their reactivity toward hydroxyl radicals (see Materials and Methods). This technique reveals the solvent-protected core of the docked conformation at nucleotide resolution by protection from hydroxyl radicals generated in solution (*9*). Consistent with our trFRET results, we found the same residues (G11 to A15, C25 to C27 and A38, U42-A43, C-2 to G/U+2) protected in the 5′- and 3′-segments of WT and mutant two-strand ribozyme−substrate complexes, in the presence of both Mg^{2+} and $Co(NH_3)_6^{3+}$ [Figure 3(b)]. Within the resolution limits of the utilized techniques, we can therefore conclude that U+2 base substitutions result in a specifically and stably docked conformation similar to that of the WT complex. The folding transition, however, is kinetically more complex than that observed with the WT substrate.

Domain Docking Involves Unstacking of Base +2. 2-Aminopurine (AP) has recently been utilized as a fluorescent probe for the local dynamics of RNA bases (*32*, *33*). To monitor structural changes around the cleavage site, we incorporated commercially available 2′-O-methylated AP ribonucleoside into substrate positions −1, +1, or +2, and monitored temporal changes in AP steady-state fluorescence upon addition of ribozyme (see Materials and Methods). While the G+1→AP substrate did not lead to any fluorescence change, consistent with our observation that this modification interferes with both docking and cleavage activity of the hairpin ribozyme (see above), the A-1→AP mutant substrate showed a slight fluorescence decrease upon docking of its ribozyme−substrate complex [Figure 4(a)]. We observed by far the most significant fluorescence change, however, for the U+2→AP substrate, in which case fluo-

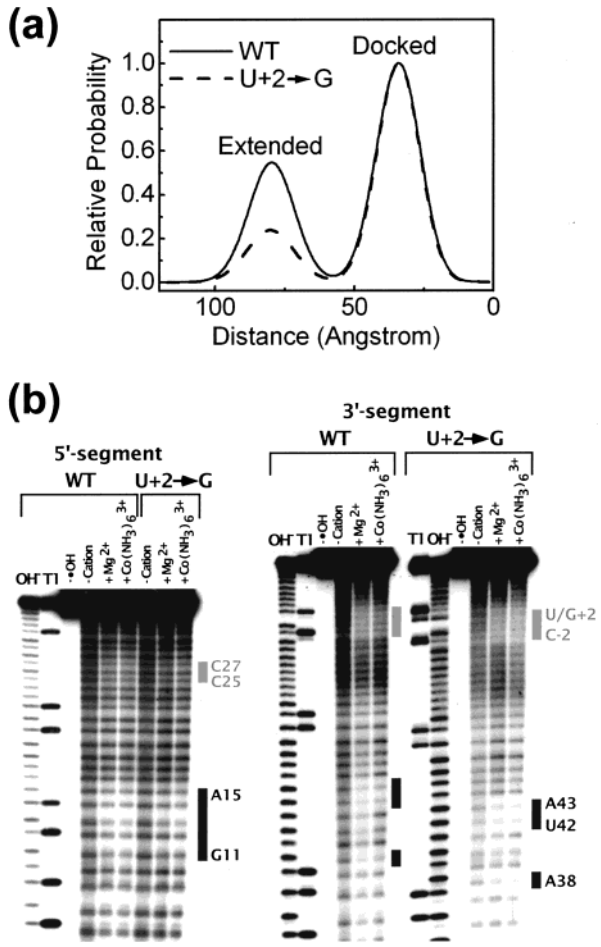

FIGURE 3: Comparison of the docked conformers of the wild-type (WT) and U+2→G mutant hairpin ribozyme−substrate complexes. (a) Normalized donor−acceptor distance distributions for the WT (solid line) and mutant (dashed line) ribozyme−substrate complexes as measured by trFRET in standard buffer at 17.8 °C (see Materials and Methods) (*10*). While the distance distributions of the extended (mean distance: 78 ± 1 Å) and docked (mean distance: 34 ± 1 Å) conformers are indistinguishable, the relative abundance of docked complex increases from 65 ± 1% to 81 ± 1% upon introducing the U+2→G mutation, equivalent to 0.5 kcal/mol additional stabilization energy. (b) Solvent-protected core of WT and U+2→G mutant ribozyme−substrate complexes as observed by hydroxyl-radical footprinting (see Materials and Methods) (*9*). Both the 5′- and 3′-segments of the two-strand WT and U+2→G mutant ribozyme−substrate complexes were analyzed in the absence (−) and presence (+) of 12 mM Mg^{2+} and 1.5 mM $Co(NH_3)_6^{3+}$, as indicated, together with a control without hydroxyl radicals (−·OH). Partial hydrolysis with alkali (OH^-) and ribonuclease T1 (shifted up by one nucleotide compared to the hydroxyl radical pattern) (*9*) served to identify protected areas, highlighted in the same shades as in Figure 1(a).

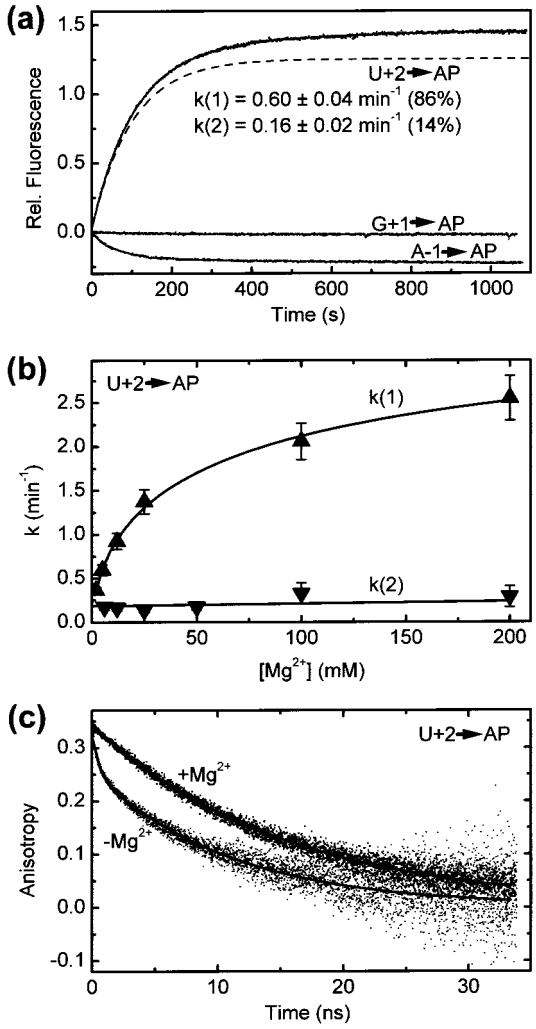

FIGURE 4: Analysis of a localized structural change involving the +2 substrate position and accompanying docking, using 2-aminopurine as a fluorescent probe. (a) Change of AP steady-state fluorescence upon docking. After formation of the ribozyme−substrate complex (containing noncleavable substrate analogues with AP in either the −1, +1, or +2 position) under standard conditions (50 mM Tris-HCl, pH 7.5, 12 mM $MgCl_2$, 25 °C), the relative change in AP fluorescence was observed; only the U+2→AP substrate led to a significant change that was fitted to a double-exponential growth function with the indicated rate constants (with errors from comparing three independent determinations) and relative amplitudes. Dashed line, contribution of the fast-phase component that alone cannot satisfy the data. (b) Mg^{2+} dependence of the two rate constants that describe the AP fluorescence increase upon docking of the U+2→AP ribozyme−substrate complex. While the slow rate constant, $k(2)$, remained essentially unchanged, the Mg^{2+} dependence of the fast rate constant, $k(1)$, could be fitted with a cooperative binding equation (see Materials and Methods) to yield an apparent Mg^{2+} dissociation constant of 74 mM and a cooperativity constant n of 0.62 (solid line). (c) Time-resolved fluorescence anisotropy decay of AP in the U+2→AP ribozyme−substrate complex, in the absence ($-Mg^{2+}$) and presence ($+Mg^{2+}$) of Mg^{2+}. Data were fitted with double- and single-exponential decay functions (solid lines, see Materials and Methods), respectively, the parameters of which are reported in Table 2.

rescence increases more than 100% [Figure 4(a)], consistent with substantial unstacking of the AP base (*27*, *32*, *33*).

Previously, it has been shown that AP incorporated into a nucleic acid chain exhibits four distinct fluorescence lifetimes that represent different base stacking states (*27*); the longest lifetime, typically around 10 ns, is indicative of a completely unstacked base, the shortest lifetime (typically 50−90 ps) reflects a strongly stacked AP, and the two intermediate lifetimes represent bases in the population with partial stacking interactions. We found that the only AP-containing substrate that, upon domain docking in the presence of Mg^{2+}, undergoes a substantial distribution shift toward the longest lifetime component is the U+2→AP substrate (Table 2). This observation further corroborates the notion that AP+2 unstacks upon tertiary structure folding.

The kinetics of this local unstacking event are biphasic and share similar rate constants with global docking of this ribozyme−substrate complex as observed by FRET [compare Figures 2 and 4(a)]. To test whether AP+2 unstacking and

domain docking are coupled, we observed the kinetics of the AP+2 fluorescence change over a wide range of Mg^{2+} concentrations [Figure 4(b)]. Throughout this range, the fast-phase rate constant matches that for global domain docking as previously measured by FRET (*8*), suggesting that AP+2 unstacking indeed is indicative of substrate straining upon domain docking (*20*). We note that this is evidence for quasi-hierarchical folding in the hairpin ribozyme (*3*). The slow-phase rate constant is Mg^{2+}-independent, possibly an indication that the associated process may not be electrostatically driven (*34, 35*).

Domain Docking Results in Restricted AP+2 Conformational Dynamics. The fluorescence anisotropy decay of AP directly reports on the conformational dynamics of the base; it can be caused by both local rotation of the base, which occurs on the subnanosecond time scale, and overall rotational diffusion of the complex that the base is incorporated in, which typically is of a nanosecond time scale (*27*). We compared the fluorescence anisotropy decay of the U+2→AP mutant ribozyme−substrate complex in the absence and presence of Mg^{2+} [Figure 4(c)] and found that a fast-decay component of 420 ps is lost upon domain docking in the presence of Mg^{2+}; allowing for a fast component improved the exponential decay fit for the "$-Mg^{2+}$" data set considerably, while it did not improve the fit for the "$+Mg^{2+}$" data set (Table 2). We therefore conclude that the local conformational dynamics of AP+2 become restricted upon tertiary structure formation, so that its fluorescence anisotropy can only decay through the slow overall rotational diffusion pathway.

A Nativelike Trap. Folding of large catalytic RNAs is often characterized by intermediates bearing nonnative interactions that pose kinetic folding traps on or off the pathway toward the native structure (*3*). An indication for such a trap is the accelerated formation of the catalytically active structure upon addition of a denaturant like urea. In the hairpin ribozyme, the metastable extended conformation [Figure 1(b)] represents such a kinetic folding trap as the addition of 2 M urea increases the cleavage rate of the WT substrate about 4-fold (P. A. Chan and N. G. Walter, unpublished results). However, cleavage of the U+2→G mutant substrate is not notably enhanced in 2 M urea (data not shown), suggesting that escape from the kinetic folding trap posed by the extended conformation does not contribute to the observed slow cleavage of the substrate. The pH dependence of the cleavage rate of the U+2→G mutant substrate is small [it increases by only about 2-fold between pH 6.5 and pH 8.5 (data not shown)], as is that of the WT substrate, consistent with the notion that the rate-limiting step in both cases either does not involve a proton transfer or involves at least two proton transfers whose effects on the reaction rate cancel out (*36*).

What slows down cleavage of the U+2 mutant substrates? U+2, despite being preferred, is not absolutely required for cleavage, since an abasic site still leads to significant cleavage activity. Hence, it is unlikely to play a direct role in reaction chemistry, and its mutation most likely interferes with proper structure formation. In the NMR structure of the isolated loop A of the hairpin ribozyme, U+2 was found to be in a dynamic conformational exchange, and was assigned to be bulged out (*15*). In molecular modeling studies based on domain cross-linking, a conformational rearrangement of U+2 into the minor groove was proposed to occur upon domain docking (*17*). Such a localized conformational transition upon docking also has been suggested based on changes in the circular dichroism and chemical reactivity of thiocarbonyl-substituted uracils (*22*).

Here, we have directly observed a docking-induced conformational change at the +2 position using an AP substitution. Our fluorescence data suggest that U+2→N substitutions stabilize a docked conformation in which the +2 base, at least in the case of AP+2, unstacks from other bases, yet becomes conformationally restricted. Our trFRET and hydroxyl-radical footprinting data indicate that the docked conformer of the mutant ribozyme−substrate complexes has the same interdomain distance and specific solvent-inaccessible core as the wild-type complex; i.e., it is nativelike. A plausible explanation for these observations is that bases substituting U+2 establish hydrogen bonds that stabilize a nativelike conformation, yet have to be broken for the complex to proceed to the chemical transition state [Figure 1(b)]. In other words, only a uracil in position +2 would make the correct and/or avoid incorrect structural contacts for the complex to cleave rapidly, while all other bases in position +2 fail to do so for steric or geometric reasons. Consistent with this model, the additional stabilization energy found by trFRET for the docked conformer involving the U+2→G mutant substrate is of the same magnitude as its additional transition state enthalpy [0.5 kcal/mol; Figure 3(a) and Table 1; although $\Delta H^{\ddagger}$ can only be defined with some uncertainty]. This proposed mechanism for interference of a single base substitution with catalytic activity is distinct from that observed in large catalytic RNAs (*5*−*7*), or the wild-type hairpin ribozyme itself (*8*−*10*), in which early metastable intermediates pose kinetic folding traps, slowing down native structure formation.

ACKNOWLEDGMENT

We thank David Pecchia for his expert RNA synthesis as well as the National Institutes of Health for grant support to D.P.M. and J.M.B.

REFERENCES

1. Brion, P., and Westhof, E. (1997) *Annu. Rev. Biophys. Biomol. Struct. 26*, 113−137.
2. Tinoco, I., Jr., and Bustamante, C. (1999) *J. Mol. Biol. 293*, 271−281.
3. Treiber, D. K., and Williamson, J. R. (1999) *Curr. Opin. Struct. Biol. 9*, 339−345.
4. Chen, S. J., and Dill, K. A. (2000) *Proc. Natl. Acad. Sci. U.S.A. 97*, 646−651.
5. Treiber, D. K., Rook, M. S., Zarrinkar, P. P., and Williamson, J. R. (1998) *Science 279*, 1943−1946.
6. Rook, M. S., Treiber, D. K., and Williamson, J. R. (1998) *J. Mol. Biol. 281*, 609−620.
7. Pan, J., Deras, M. L., and Woodson, S. A. (2000) *J. Mol. Biol. 296*, 133−144.
8. Walter, N. G., Hampel, K. J., Brown, K. M., and Burke, J. M. (1998) *EMBO J. 17*, 2378−2391.
9. Hampel, K. J., Walter, N. G., and Burke, J. M. (1998) *Biochemistry 37*, 14672−14682.
10. Walter, N. G., Burke, J. M., and Millar, D. P. (1999) *Nat. Struct. Biol. 6*, 544−549.
11. Walter, N. G., and Burke, J. M. (1998) *Curr. Opin. Chem. Biol. 2*, 24−30.
12. Murchie, A. I., Thomson, J. B., Walter, F., and Lilley, D. M. (1998) *Mol. Cell 1*, 873−881.

13. Fedor, M. J. (2000) *J. Mol. Biol. 297*, 269−291.
14. Welch, P. J., Barber, J. R., and Wong-Staal, F. (1998) *Curr. Opin. Biotechnol. 9*, 486-496.
15. Cai, Z., and Tinoco, I. (1996) *Biochemistry 35*, 6026−6036.
16. Butcher, S. E., Allain, F. H., and Feigon, J. (1999) *Nat. Struct. Biol. 6*, 212−216.
17. Earnshaw, D. J., Masquida, B., Muller, S., Sigurdsson, S. T., Eckstein, F., Westhof, E., and Gait, M. J. (1997) *J. Mol. Biol. 274*, 197−212.
18. Pinard, R., Heckman, J. E., and Burke, J. M. (1999) *J. Mol. Biol. 287*, 239−251.
19. Pinard, R., Lambert, D., Walter, N. G., Heckman, J. E., Major, F., and Burke, J. M. (1999) *Biochemistry 38*, 16035−16039.
20. Fersht, A. (1999) *Structure and Mechanism in Protein Science*, W. H. Freeman, New York.
21. Shippy, R., Siwkowski, A., and Hampel, A. (1998) *Biochemistry 37*, 564−570.
22. Komatsu, Y., Kumagai, I., and Ohtsuka, E. (1999) *Nucleic Acids Res. 27*, 4314−4323.
23. Perez-Ruiz, M., Barroso-DelJesus, A., and Berzal-Herranz, A. (1999) *J. Biol. Chem. 274*, 29376−29380.
24. Walter, N. G., and Burke, J. M. (2000) *Methods Enzymol. 317*, 409−440.
25. Esteban, J. A., Banerjee, A. R., and Burke, J. M. (1997) *J. Biol. Chem. 272*, 13629−13639.
26. Eis, P. S., and Millar, D. P. (1993) *Biochemistry 32*, 13852−13860.
27. Guest, C. R., Hochstrasser, R. A., Sowers, L. C., and Millar, D. P. (1991) *Biochemistry 30*, 3271−3279.
28. Chowrira, B. M., Berzal-Herranz, A., and Burke, J. M. (1991) *Nature 354*, 320−322.
29. Grasby, J. A., Mersmann, K., Singh, M., and Gait, M. J. (1995) *Biochemistry 34*, 4068−4076.
30. Walter, N. G., Albinson, E., and Burke, J. M. (1997) *Nucleic Acids Symp. Ser. 36*, 175−177.
31. Klostermeier, D., and Millar, D. P. (2000) *Biochemistry 39*, 12970−12978.
32. Millar, D. P. (1996) *Curr. Opin. Struct. Biol. 6*, 322−326.
33. Menger, M., Eckstein, F., and Porschke, D. (2000) *Biochemistry 39*, 4500−4507.
34. Buchmueller, K. L., Webb, A. E., Richardson, D. A., and Weeks, K. M. (2000) *Nat. Struct. Biol. 7*, 362−366.
35. Russell, R., Millett, I. S., Doniach, S., and Herschlag, D. (2000) *Nat. Struct. Biol. 7*, 367−370.
36. Nakano, S., Chadalavada, D. M., and Bevilacqua, P. C. (2000) *Science 287*, 1493−1497.
37. Porschke, D., Burke, J. M., and Walter, N. G. (1999) *J. Mol. Biol. 289*, 799−813.
38. Fedor, M. J. (1999) *Biochemistry 38*, 11040−11050.

BI001609F